Cloud Geometry Effects on Atmospheric Solar Absorption

QIANG FU AND M. C. CRIBB

Department of Oceanography, Dalhousie University, Halifax, Nova Scotia, Canada

H. W. BARKER

Atmospheric Environment Service, Downsview, Ontario, Canada

S. K. KRUEGER

Department of Meteorology, University of Utah, Salt Lake City, Utah

A. GROSSMAN

Atmospheric Sciences Division, Lawrence Livermore National Laboratory, Livermore, California

(Manuscript received 11 June 1998, in final form 31 March 1999)

ABSTRACT

A 3D broadband solar radiative transfer scheme is formulated by integrating a Monte Carlo photon transport algorithm with the Fu–Liou radiation model. It is applied to fields of tropical mesoscale convective clouds and subtropical marine boundary layer clouds that were generated by a 2D cloud-resolving model. The effects of cloud geometry on the radiative energy budget are examined by comparing the full-resolution Monte Carlo results with those from the independent column approximation (ICA) that applies the plane-parallel radiation model to each column.

For the tropical convective cloud system, it is found that cloud geometry effects always enhance atmospheric solar absorption regardless of solar zenith angle. In a large horizontal domain (512 km), differences in domain-averaged atmospheric absorption between the Monte Carlo and the ICA are less than 4 W m^{-2} in the daytime. However, for a smaller domain (e.g., 75 km) containing a cluster of deep convective towers, domain-averaged absorption can be enhanced by more than 20 W m^{-2}. For a subtropical marine boundary layer cloud system during the stratus-to-cumulus transition, calculations show that the ICA works very well for domain-averaged fluxes of the stratocumulus cloud fields even for a very small domain (4.8 km). For the trade cumulus cloud field, the effects of cloud sides and horizontal transport of photons become more significant. Calculations have also been made for both cloud systems including black carbon aerosol and a water vapor continuum. It is found that cloud geometry produces no discernible effects on the absorption enhancement due to the black carbon aerosol and water vapor continuum.

The current study indicates that the atmospheric absorption enhancement due to cloud-related 3D photon transport is small. This enhancement could not explain the excess absorption suggested by recent studies.

1. Introduction

The absorption of solar radiation by the earth–atmosphere system is the prime physical process that drives atmospheric circulation and ocean currents. While solar energy absorbed by the system can be derived directly from satellite measurements (e.g., Barkstrom 1984; Kyle et al. 1993), its partition between the atmosphere and surface, which is also an important factor in determining the earth's climate (e.g., Kiehl et al. 1995), remains uncertain at all scales. This is largely because the effect of clouds on atmospheric solar absorption is still not well understood (e.g., Stephens and Tsay 1990).

Radiation schemes used in general circulation models (GCMs) indicate that clouds have little effect on globally averaged atmospheric solar absorption (e.g., Li et al. 1993). Recently, several observational studies (Cess et al. 1995; Ramanathan et al. 1995; Pilewskie and Valero 1995) suggest that clouds may enhance the global mean atmospheric absorption by ~25 W m^{-2}. The magnitude of this discrepancy and its explanation are, however, a subject of much debate and uncertainty (e.g., Li et al. 1995; Wiscombe 1995; Stephens 1996; Arking 1996).

Corresponding author address: Prof. Qiang Fu, Atmospheric Science Program, Dept. of Oceanography, Dalhousie University, Halifax, NS B3H 4J1, Canada.
E-mail: qfu@atm.dal.ca

Clouds often exhibit complex structure in all directions. Thus, it has been hypothesized that this absorption anomaly may stem from the fact that in conventional radiative transfer calculations, a cloud field is usually treated as series of isolated, plane-parallel columns. This method is known as the independent column approximation (ICA). Byrne et al. (1996) argue that broken cloud fields may cause average photon pathlengths to be longer than those predicted by plane-parallel radiative transfer calculations, especially under and within the clouds, which contributes to excess cloud absorption. O'Hirok and Gautier (1998) also suggest that the assumption of plane-parallel clouds cannot be excluded as one of the major factors behind the cloud absorption enhancement, especially for tropical cloud fields. Barker et al. (1998), however, show that domain-averaged atmospheric absorption of solar radiation within a typical GCM grid cell depends very weakly on cloud geometry.

Herein a three-dimensional (3D) broadband solar radiative transfer algorithm is formulated by combining a 3D Monte Carlo photon transport scheme (Barker 1991) with the radiation model developed by Fu and Liou (1992, 1993). This algorithm is used to investigate the effect of cloud geometry on the radiative energy budget. Two typical cloud systems, tropical mesoscale convective clouds and subtropical marine boundary layer clouds, are considered; both cloud systems were generated by a cloud-resolving model (CRM) (Fu et al. 1995, hereinafter FKL; Krueger et al. 1995, hereinafter KMF). Of primary concern here is the 3D effect of clouds on the atmospheric absorption of solar radiation. Moreover, black carbon aerosol and the water vapor continuum are included to determine whether their impact on total atmospheric absorption depends on assumptions made about cloud geometry.

This paper is organized as follows. Section 2 presents a brief description of the two cloud systems used in this study. Section 3 describes the radiation models used, and section 4 presents numerical results. In section 5, results pertaining to black carbon aerosol and to the water vapor continuum are discussed. Summary and conclusions are given in section 6.

2. Cloud fields

Cloud fields produced from the University of Utah cloud resolving model (UU CRM) are used. This model has been described in detail previously (Krueger 1988; Xu and Krueger 1991; FKL, KMF). Dynamics are represented explicitly and governed by a set of two-dimensional (x–z) anelastic equations. The resulting mesoscale and cloud-scale dynamical equations are coupled with a third-moment turbulence closure. The CRM also includes a turbulent-scale condensation scheme, a surface flux parameterization based on flux–profile relationships, and a bulk microphysics parameterization. The cyclic lateral boundary condition is used, and the large-scale forcing is based on climatological data.

a. Tropical convective cloud system

The life cycle of a tropical squall line was simulated by FKL using thermodynamic and kinematic initial conditions as well as large-scale advective forcing typical of a Global Atmospheric Research Program (GARP) Atlantic Tropical Experiment phase III squall cluster environment. Since tropical anvils associated with a mesoscale convective system are about 200 km wide, FKL used a horizontal domain of 512 km with a grid size of 1 km. The depth of the domain is about 18 km and contains 34 layers of variable geometric thickness. Hydrometeors in the CRM are categorized into five types: cloud droplets, ice crystals, raindrops, snow, and graupel.

Cloud fields at the developing, mature, and dissipating stages of the mesoscale convective system are considered. They are from the R3 simulation at 120, 325, and 645 min (FKL). Figure 1 shows snapshots for these cloud fields using the total hydrometeor content (g m^{-3}), including cloud water, cloud ice, rain, snow, and graupel. In the developing stage (Fig. 1a), the cloud cluster consists of isolated precipitating convective towers. In the mature stage (Fig. 1b), the anvil cloud associated with the mesoscale convective system extends horizontally for more than 150 km. In the dissipating stage (Fig. 1c), the upper-tropospheric stratiform clouds are thinning and breaking up.

Tropical cloud fields were also used in the studies by O'Hirok and Gautier (1998) and Barker et al. (1998); both considered only liquid cloud water, though 3D clouds were used. In O'Hirok and Gautier (1998), cloud geometry was synthesized from cloud-top heights derived from satellite imagery with ad hoc additions. Liquid water content in the vertical was based on the adiabatic process while remaining constant along the horizontal plane within a cloud. In Barker et al. (1998), the cloud field was produced from a cloud-resolving model, but ice, rain, snow, and graupel concentrations were neglected. In this aspect, the cloud fields shown in Fig. 1 are more realistic. Note that the clouds in this study are two-dimensional, but this does not affect the generality of our results.

b. Subtropical marine boundary clouds

The areal extent and general longevity of marine stratocumulus clouds make them an important component of the earth's climate system since they can increase the albedo over large tracts of ocean (Albrecht et al. 1988). Typical of the eastern and equatorward quadrants of the subtropical high-pressure zones, a transition occurs from a stratus-topped boundary layer to a trade cumulus boundary layer. The change in cloud cover could modify both the albedo and the solar flux reaching the ocean.

A stratus-to-cumulus transition was generated in a Lagrangian simulation following the evolution of the boundary layer as it moved from the California coast

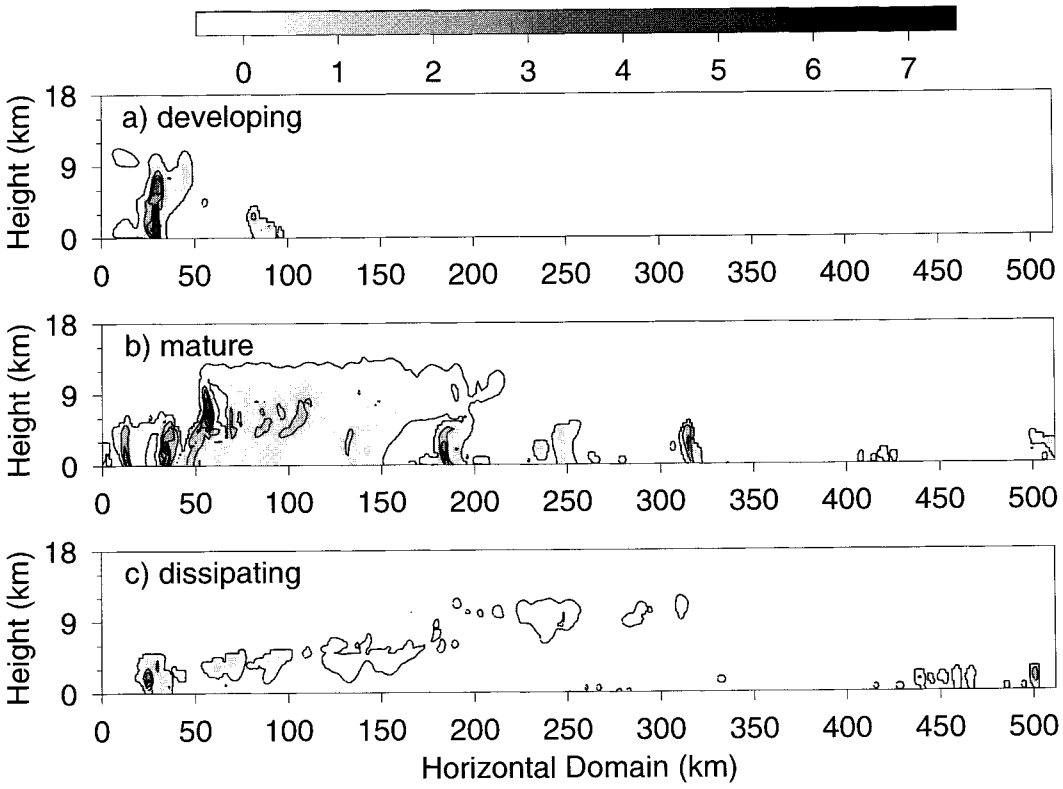

FIG. 1. Cloud fields for the (a) developing, (b) mature, and (c) dissipating stages of a tropical mesoscale convective squall line system. These fields are the total hydrometeor content (g m^{-3}), including cloud ice, cloud water, rain, snow, and graupel. Contours shown are as in the increments of the grayscale.

to Hawaii during July (KMF). This transition involves a radical decrease in cloud amount from overcast stratus to scattered cumulus in the boundary layer. In the CRM simulation, the horizontal domain is 4.8 km with a grid size of 75 m. The vertical domain is 3 km with a resolution of 50 m.

The cloud fields at 24, 72, and 120 h were selected for this study, which are stratocumulus (Sc), cumulus under stratocumulus (Cu under Sc), and the trade cumulus (Cu) cloud fields. Figure 2 shows snapshots of cloud liquid water content of these fields.

3. Radiation models

In the solar spectrum, the absorption and scattering processes in the atmosphere are characterized by the single-scattering properties of particles and molecules, namely, the extinction coefficient, single-scattering albedo, and the scattering phase function. Optical properties associated with cloud water, cloud ice, rain, snow, and graupel are calculated following Fu and Liou (1993) and Fu et al. (1995). Parameterization of Rayleigh scattering is included. Using the HITRAN database, nongray gaseous absorption due to H_2O, CO_2, O_3, O_2, CH_4, and N_2O is parameterized based on the correlated *k*-distribution approach (Fu and Liou 1992). The absorption by O_3 in the UV–visible regions, including the Hartley, Huggins, and Chappuis bands, is also included (Fu 1991). The combined single-scattering properties are obtained using the mixing rule (Fu and Liou 1993) for each CRM grid box, which are used in both plane-parallel and 3D radiative transfer schemes. In the present code, the solar spectrum is divided into six bands, and 54 spectral calculations are required for broadband radiative transfer simulations.

a. Independent column approximation

In the ICA (e.g., Cahalan et al. 1994a), radiative fluxes are computed on a column-by-column basis with plane-parallel radiative transfer theory. The ICA is a standard approach used in CRMs (e.g., FKL; KMF). Since the ICA performs plane-parallel calculations for each column, it neglects horizontal photon transport between columns. As the cloud distributions used in both ICA and 3D transfer models are exactly the same, differences between the ICA and 3D results can be attributed to the plane-parallel assumption (O'Hirok and Gautier 1998; Barker et al. 1998). Examining the validity of the ICA is also meaningful since time series of observed cloud profiles are becoming available through ground-based microwave radiometers and millimeter radars (e.g., Mace et al. 1998; Zuidema and Evans 1998).

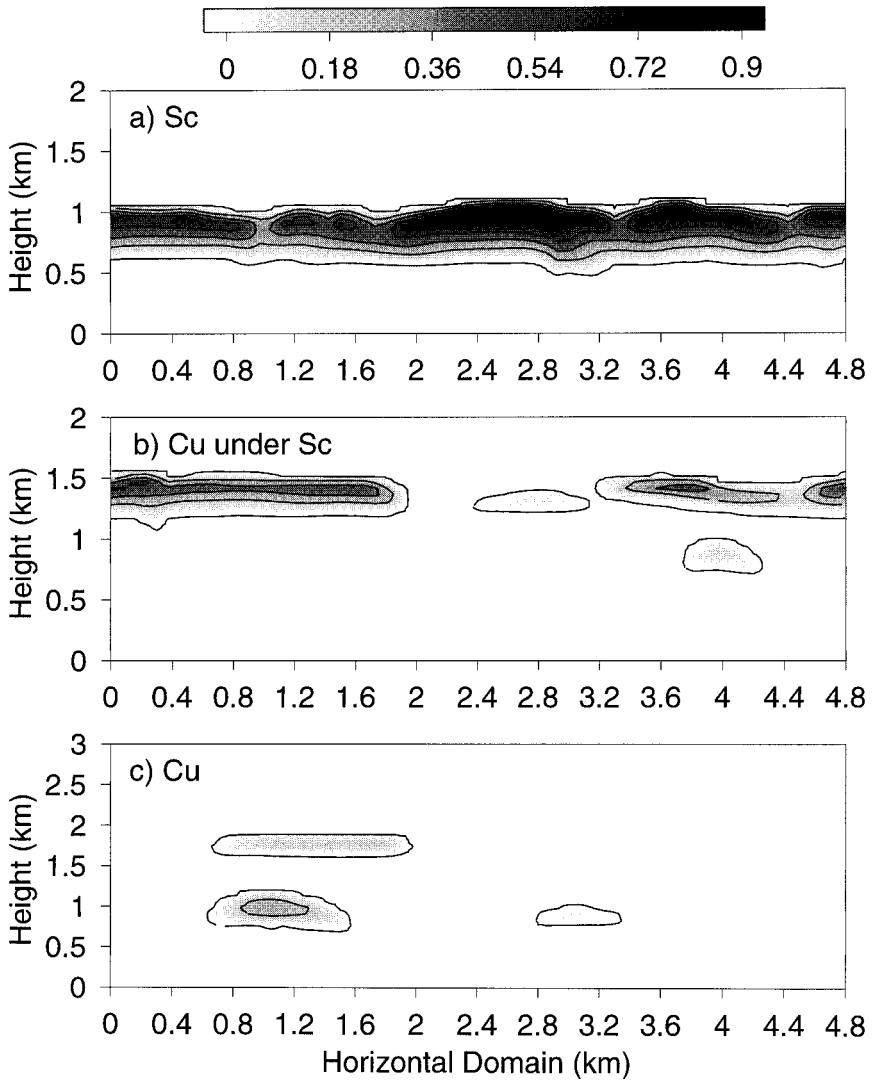

FIG. 2. Cloud liquid water content (g m^{-3}) for the (a) Sc, (b) Cu under Sc, and (c) the trade Cu cloud fields during the stratus-to-cumulus transition in the subtropical marine boundary layer. Contours shown are as in the increments of the grayscale.

The plane-parallel radiative transfer scheme used here is the delta-four-stream approximation (Liou et al. 1988). For applications of the delta-four-stream to vertically nonhomogeneous atmospheres, the atmosphere is divided into a number of homogeneous layers, and the internal continuity requirement of diffuse intensities is used (Fu and Liou 1993). Compared with the delta-128-stream scheme under different atmospheric conditions, errors in atmospheric solar absorption due to the delta-four-stream approximation are less than ~0.3 W m^{-2}.

b. The 3D Monte Carlo radiative transfer algorithm

Given the distribution of single-scattering properties in the atmosphere, the 3D transport of photons can be modeled accurately by the Monte Carlo technique. In this technique, the atmosphere is divided into a 3D lattice of elementary rectangular cells, and single-scattering properties are assigned to each homogeneous cell. Both the trajectory and weight of each photon are traced through the lattice until the photon either exits the top of the domain or its weight falls below a predefined threshold. Thus, this method can yield flux and absorption estimates for a specific 3D cloud field. The 3D Monte Carlo code developed by Barker (1991) was used throughout. This study makes exclusive use of cyclic atmospheric and photon trajectory boundary conditions. The surface is modeled as a Lambertian reflector.

Using the single-scattering parameterization developed by Fu and Liou, a number of monochromatic radiative transfer calculations are needed to obtain solar broadband fluxes. If N photons are injected into the system, the number of photons for each spectral cal-

TABLE 1. Atmospheric absorption of solar radiation in the midlatitude summer atmosphere under various cloud conditions and at different solar zenith angles (θ). Delta-four-stream (D4S) and Monte Carlo (MC) calculations, as well as the differences (Δ), are shown. The surface albedo is 0.05; five million photons are used in the MC simulation. Units are W m^{-2}.

Atmospheric conditions	θ	Atmospheric absorption		
		MC	D4S	Δ
Clear	30	200.4	200.2	0.2
	60	135.5	135.3	0.2
	75	84.6	84.5	0.1
Low	30	276.1	276.0	0.1
	60	161.3	161.9	−0.6
	75	89.3	89.5	−0.2
Middle	30	251.2	252.0	−0.8
	60	136.1	136.5	−0.4
	75	70.5	70.2	0.3
High	30	203.9	203.9	0.0
	60	130.1	130.1	0.0
	75	71.8	71.9	−0.1
Low, middle, and high	30	261.9	262.1	−0.2
	60	141.2	141.4	−0.2
	75	71.4	71.0	0.4

culation is Nf_i, where f_i is the fraction of total solar energy contained in that spectral band ($\sum_{i=1}^{54} f_i = 1$). Thus, computer time required for broadband calculations is independent of the number of spectral intervals. Since photon weight is decreased due to absorption after each scattering event, computer time is saved by terminating photons when their weight is smaller than 10^{-5}.

The 3D Monte Carlo broadband radiation code is first assessed in a plane-parallel atmosphere. Broadband flux and heating rate calculations are made using the midlatitude summer atmosphere (McClatchey et al. 1971) at a vertical spacing of 0.25 km, a surface albedo of 0.05, and solar zenith angles of 30°, 60°, and 75°. Conditions used are clear sky; cloudy sky with a low, middle, or high cloud layer; and a sky with all three cloud layers. The low cloud layer is 1-km thick with a base height of 1 km, a liquid water content of 0.22 g m^{-3}, and an effective radius of 5.89 μm. The middle cloud layer is 2-km thick with its base placed at 5 km, liquid water content is 0.47 g m^{-3}, and effective radius is 9.84 μm. Extending from 10 to 12 km above the surface, the high cloud layer has an ice water content of 4.8×10^{-3} g m^{-3}, and the mean effective size of ice crystals is 41.5 μm. Table 1 summarizes total atmospheric absorption of solar radiation from the delta-four-stream and the 3D Monte Carlo radiation models. Differences between estimates from the two approaches are less than 0.3 W m^{-2} for the majority of the cases.

c. Mixing rule

In our plane-parallel and 3D radiative transfer schemes, the single-scattering properties for each elementary homogeneous cell are obtained by combining optical properties associated with the cloud particles and gases based on the mixing rule (Fu and Liou 1993). Use of this rule is a common practice in conventional radiation models. However, in the Monte Carlo radiative transfer algorithms developed by O'Hirok and Gautier (1998) and Barker et al. (1998), the attenuations by cloud droplets and gases are treated separately. In this section, the validity of the mixing rule is examined.

Consider a homogeneous layer where the extinction by cloud droplets is mixed with the gaseous absorption. For simplicity, cloud particles are assumed to be nonabsorbing. Treating the scattering by cloud droplets and the absorption by the gas separately (hereinafter, method I), the absorption of the layer can be expressed in the form (Barker et al. 1998),

$$A = 1 - \frac{1}{N}\sum_{i=1}^{N} e^{-\beta_a l_i}, \tag{3.1}$$

where β_a is the absorption coefficient of the gas, N the number of photons injected into the system, and l_i the total pathlength of a given photon in the layer before exiting. Assume that the extinction coefficient of the droplets is β_c. The photon free-pathlength between scattering events is determined by

$$f_p = -\ln(R)/\beta_c, \tag{3.2}$$

where R is a random number uniformly distributed on (0, 1). Thus the photon mean free-pathlength is $1/\beta_c$.

Using the mixing rule (hereinafter, method II), the combined extinction coefficient and single-scattering albedo for the homogeneous layer are $\beta_a + \beta_c$ and $\beta_c/(\beta_a + \beta_c)$, respectively. In this case the photon mean free-pathlength is $1/(\beta_a + \beta_c)$. The absorption of the layer can be written as

$$A = 1 - \frac{1}{N}\sum_{i=1}^{N} \left(\frac{\beta_c}{\beta_a + \beta_c}\right)^{n_i}, \tag{3.3}$$

where n_i is the total number of scattering events before the photon exits the layer.

Since different mean free-pathlengths are obtained using these two treatments, the statistics for the total number of scattering events and photon total pathlengths from methods I and II are quite different. Here we cannot show mathematically that Eqs. (3.1) and (3.3) are equivalent. However, our numerical experiments demonstrate that the absorption using method I is exactly the same as that based on method II. In the numerical experiments, we have considered the total optical depth ($\tau_c + \tau_a$) ranging from 10^{-2} to 10^2, combined single-scattering albedo [$\tau_c/(\tau_c + \tau_a)$] from 0 to 1, and asymmetry factor from 0 to 1.

This result can be understood as follows. We first consider the layer containing only the absorbing gas. Based on method I, f_p would be infinity, and photons would pass through the layer without experiencing any scattering events. Therefore, the absorption of the layer is $1 - e^{-\beta_a z/\mu_0}$, where z is the thickness of the layer and

TABLE 2. Domain-averaged solar upward fluxes at the top of the atmosphere ($\overline{F}^{\uparrow}_{\mathrm{TOA}}$), domain-averaged solar downward fluxes at the surface ($\overline{F}^{\downarrow}_{\mathrm{SFC}}$), and the domain-averaged absorption in the atmosphere for the three stages in the life cycle of the tropical convective cloud system. The ICA and 3D Monte Carlo calculations at different solar zenith angles (θ) are presented, along with the differences (Δ). Units are W m^{-2}.

		$\overline{F}^{\uparrow}_{\mathrm{TOA}}$			$\overline{F}^{\downarrow}_{\mathrm{SFC}}$			$\overline{A}$		
Cloud stages	θ	3D	ICA	$\Delta\overline{F}^{\uparrow}_{\mathrm{TOA}}$	3D	ICA	$\Delta\overline{F}^{\downarrow}_{\mathrm{SFC}}$	3D	ICA	$\Delta\overline{A}$
Developing	0	167.1	171.7	−4.6	977.2	973.5	3.7	264.9	263.8	1.1
	30	156.4	157.8	−1.4	824.9	825.8	−0.9	238.0	235.7	2.3
	60	113.3	111.5	1.8	433.5	437.3	−3.8	155.0	153.2	1.8
	75	73.9	71.6	2.3	194.8	198.7	−3.9	93.1	91.7	1.4
Mature	0	428.7	449.1	−20.4	659.8	640.8	19.0	304.8	302.4	2.4
	30	392.9	404.7	−11.8	546.0	536.0	10.0	266.5	264.2	2.3
	60	265.1	265.6	−0.5	266.6	270.1	−3.5	161.8	158.0	3.8
	75	158.8	153.8	5.0	108.7	117.1	−8.4	90.0	87.0	3.0
Dissipating	0	272.4	277.5	−5.1	859.2	854.5	4.7	271.7	271.0	0.7
	30	254.8	256.7	−1.9	717.4	716.5	0.9	241.7	240.7	1.0
	60	183.7	183.4	0.3	360.9	362.8	−1.9	153.6	152.1	1.5
	75	118.6	114.0	4.6	152.1	157.7	−5.6	89.0	88.3	0.7

μ_0 the cosine of the solar zenith angle. Using method II, f_p becomes $-\ln(R)/\beta_a$ and the single-scattering albedo is zero. Thus we also obtain an absorption of $1 - e^{-\beta_a z/\mu_0}$. Therefore, the absorbing gaseous medium can be treated as absorbing particles. Second, if we consider the mixture of these absorbing particles and cloud droplets, we have $f_p = -\ln(R)/(\beta_a + \beta_c)$. When a scattering event occurs, the choice between the absorbing particle and droplet depends on the relative magnitudes of β_a and β_c. This is equivalent to the estimation of absorption for the layer with the combined extinction coefficient and single-scattering albedo of $[\beta_a + \beta_c, \beta_c/(\beta_a + \beta_c)]$ (Barker 1991). In summary, the Eqs. (3.1) and (3.3) are equivalent so that the mixing rule to combine the single-scattering properties is valid.

4. Model simulations and results

The ICA and 3D radiation models are applied to the simulated cloud fields presented in section 2. For the radiation calculations, several levels are added above the CRM domain to complete the atmosphere (FKL; KMF). The standard tropical ozone profile is used. The two-dimensional cloud fields from the CRM are considered to have an infinite depth of the horizontal domain size, but with the same vertical profiles.

Four solar zenith angles (0°, 30°, 60°, and 75°) are considered for each different cloud field. All 3D calculations are made at an azimuth angle of 0°, which corresponds to the sun coming in from the left in Figs. 1 and 2. The effective radius of water cloud droplets and the effective size of ice cloud particles are 10 and 50 μm, respectively; the surface albedo is 0.05; and the solar constant is set to be 1360.3 W m^{-2}. In this study, 51.2 and 6.5 million photons are used for the tropical convective system and subtropical marine boundary clouds, respectively. This implies that each column receives 10^5 photons.

a. Results for tropical convective cloud system

Domain-averaged solar upward fluxes at the top of the atmosphere $\overline{F}^{\uparrow}_{\mathrm{TOA}}$, downward fluxes at the surface $\overline{F}^{\downarrow}_{\mathrm{SFC}}$, and absorption in the atmosphere $\overline{A}$ for the three stages of the tropical convective cloud system are summarized in Table 2. The 3D and ICA results using four solar zenith angles are presented along with the differences. It is evident that the 3D effects are most enhanced in the mature stage. This is because the cloud fields associated with the developing or dissipating stages are less extensive or more horizontally homogeneous.

At overhead sun, the 3D radiation model always produces larger downward surface fluxes and smaller outgoing fluxes at the top of the atmosphere. The differences can be as large as 20 W m^{-2}. This can be attributed to the fact that the 3D transfer allows photon leakage from the sides of clouds, which leads to increased transmittance (Welch and Wielicki 1984). However, at a solar zenith angle of 75°, the ICA underestimates $\overline{F}^{\uparrow}_{\mathrm{TOA}}$ and overestimates $\overline{F}^{\downarrow}_{\mathrm{SFC}}$. Note that the sign of the differences changes at solar zenith angles between 30° and 60°. The explanation for this behavior lies in the increased interception and reflection of photons by cloud sides as well as in the reduced photon leakage as the solar zenith angle is increased.

It is seen from Table 2 that domain-averaged atmospheric solar absorption from the 3D scheme consistently exceeds ICA estimates. At the mature stage, the enhanced absorption is ~3 W m^{-2} regardless of sun angle. However, the reason for these enhancements differs for different solar zenith angles. At high sun, greater downward fluxes due to photon leakage from cloud sides increase absorption by water vapor and cloud particles in the lower atmosphere. At large solar zenith angles, direct illumination of cloud sides enhances cloud particle absorption.

Figure 3 shows domain-averaged heating rate profiles from the ICA and 3D simulations for the mature stage

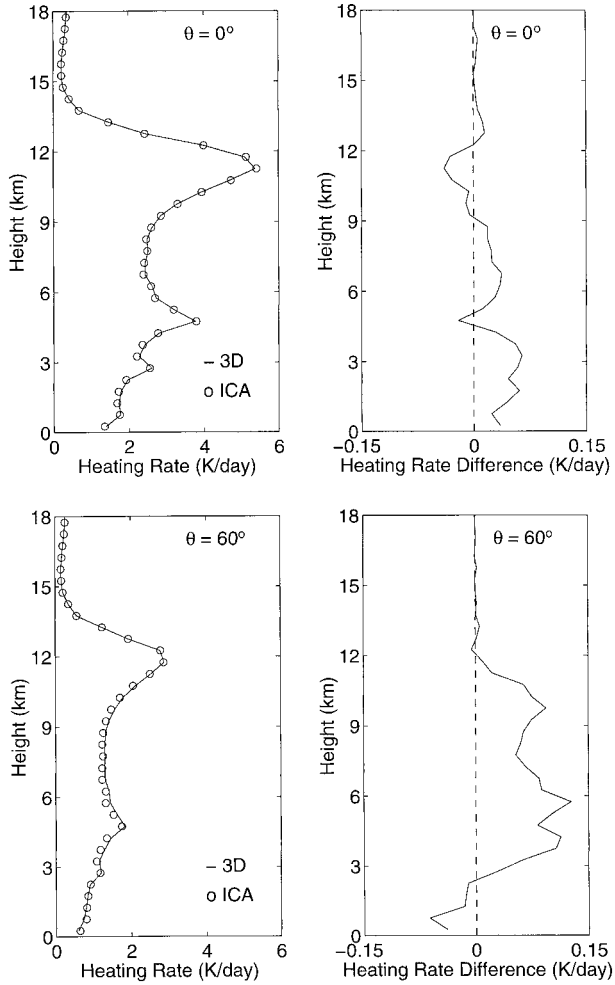

FIG. 3. Left panels show domain-averaged solar heating rate profiles computed from the 3D Monte Carlo (3D) and independent column approximation (ICA) schemes using solar zenith angles of 0° and 60°. Right panels show the corresponding differences between the 3D and ICA profiles. These plots are for the mature stage of the tropical convective system.

of the tropical convective system. The absolute difference is less than 0.12 K day^{-1}. At overhead sun, the slightly smaller heating rate around 5 and 11 km for the 3D simulation is due to the leakage of photons out of the clouds at these levels (see Fig. 1). At the solar zenith angle of 60°, the negative heating rate difference below 2.5 km is attributed to slanted shadowing of the lower atmosphere by clouds in the 3D case.

From results presented in Table 2 and Fig. 3, the impact of cloud 3D effects on the domain-averaged atmospheric absorption and heating rates is small. This result is consistent with the conclusion given by Barker et al. (1998).

It is also interesting to examine the cloud 3D effects on spatial distributions of the radiative energy budget. Figure 4 shows upward flux at 18-km altitude, downward flux at the surface, and atmospheric column absorption as functions of horizontal distance for the mature stage of the tropical convective system at a solar zenith angle of 60°. For both boundary fluxes and atmospheric absorption, the differences between the 3D and ICA calculations for a given column can easily reach several hundred W m^{-2}. Because of horizontal photon transport, the spatial variation of 3D outgoing fluxes is much smoother than that based on the ICA (Fig. 4a). Note the spikes in downward surface fluxes from the 3D case, especially for horizontal distance greater than ~250 km. From Fig. 1, it can be seen that these spikes are on the sunlit side of isolated clouds and correspond to direct-beam irradiance coupled with cloud-side reflection. For atmospheric absorption (Fig. 4c), the results from the 3D Monte Carlo scheme have a large variability associated with the deep convective cloud towers, while the absorption from the ICA is almost insensitive to the presence of clouds. The huge 3D absorption at ~55 km is due to direct illumination of solar radiation onto the side of the cloud towers that contains abundant amounts of different hydrometeors.

Compared with results from Barker et al. (1998), a more significant impact of cloud sides and horizontal transport of photons on the domain-averaged absorption was found by O'Hirok and Gautier (1998). An explanation for their results can be deduced from Fig. 4c. O'Hirok and Gautier used a horizontal domain of ~50 km that contained convective clouds derived from satellite imagery. Based on Fig. 4c for the domain from 0 to 75 km where there is a cluster of deep convective towers (Fig. 1b), the average daytime absorption derived from 3D simulation is more than 20 W m^{-2} larger than the ICA estimate. Differences for reflected and transmitted fluxes averaged over the same subdomain can be larger than 50 W m^{-2}.

Snapshots (x–z section) of solar heating rates for the mature stage at 60° are shown in Fig. 5 for the ICA and the 3D simulation. Clearly depicted are regions of intense heating near cloud walls and cloud slanted shadowing in the 3D case. Steep gradients in energy absorbed near cloud walls could have implications for cloud dynamics. The ICA case tends to concentrate its heating near cloud tops and cast vertical shadows.

Earth radiation budget measurements from space can be used to estimate the energy reflected to space. Collocated radiometers at the surface are often used to estimate transmitted radiation so that the difference between the two measurements can be approximated as the absorbed radiation in the atmospheric column. It is instructive to compare the actual atmospheric absorption and the apparent absorption, which is defined as the difference between the net fluxes at the top of the atmosphere and at the surface from the 3D simulation. The comparison is shown in Fig. 6 at solar zenith angles of 0° and 60° for the mature stage of the tropical convective cloud field. Significant and systematic error due to the residual method can be seen even when a spatial averaging is applied to a domain as large as 100 km.

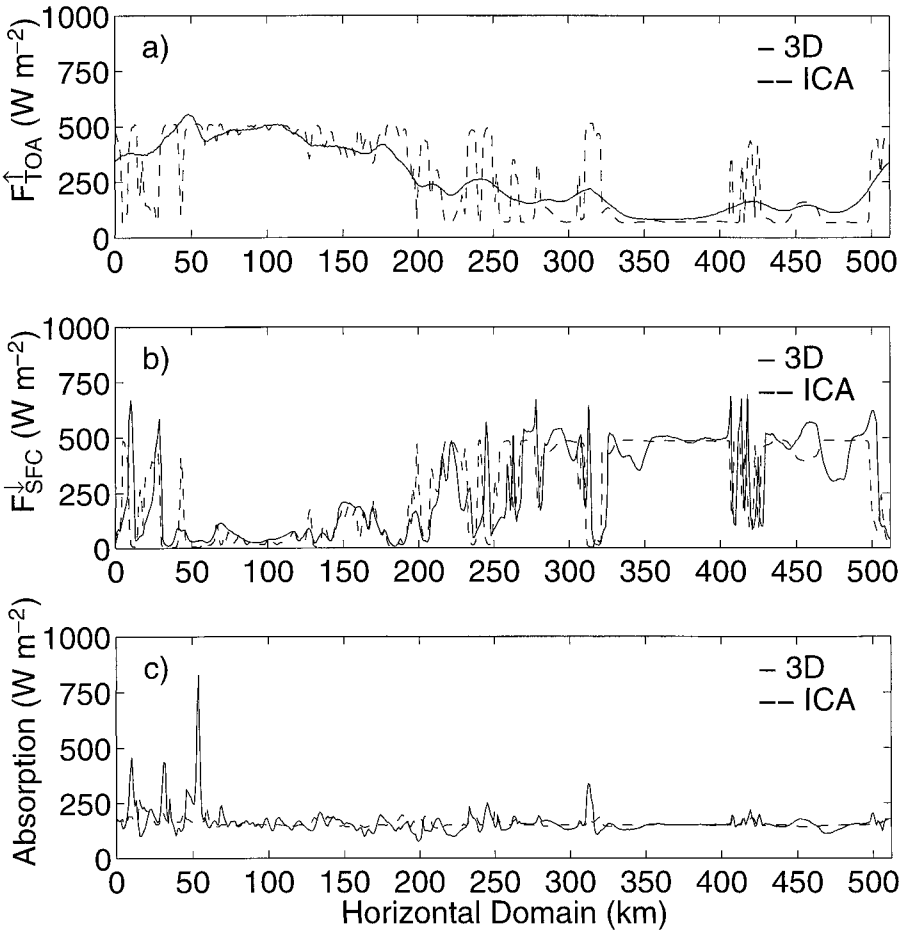

FIG. 4. (a) Solar upward flux at 18-km altitude, (b) downward flux at the surface, and (c) atmospheric column absorption as functions of horizontal distance (km) for the mature stage of the tropical convective system at a solar zenith angle of 60°. The 3D Monte Carlo (solid line) and independent-column approximation (dashed line) calculations are shown.

For tropical cloud systems, Fig. 6 demonstrates the difficulty in estimating the atmospheric absorption using the differences of net fluxes.

It is noted that the Monte Carlo results presented above are obtained when the azimuth angle is 0°. The general character of the plots is unaltered when using an azimuth angle of 180°. Using the azimuth angle of 0° or 180° versus other azimuth angles, the cloud 3D effects would be maximized, especially for a high solar zenith angle. Furthermore, note that the clouds considered here are two-dimensional, which, compared to three-dimensional cloud fields, would enhance the 3D effects when using the azimuth angle of 0°. This is because of the direct illumination of solar radiation onto the cloud-side wall associated with the 2D case.

In this study, typical cloud fields in the life cycle of a tropical convective cloud system are used to study the cloud geometry effects on the radiative energy budget. In another paper by Barker and Fu (1999), we have considered all the cloud fields generated from the cloud-resolving model, which were saved every 5 model-minutes for 10 hours, thus spanning the life cycle of the system. It is found that results derived from these three cloud fields here are representative for different stages of the system.

b. Results for subtropical marine boundary clouds

Table 3 presents the domain-averaged solar upward fluxes at the top of the atmosphere $\overline{F}^{\uparrow}_{TOA}$, downward fluxes at the surface $\overline{F}^{\downarrow}_{SFC}$, and absorption in the atmosphere $\overline{A}$ for the three stages during the stratus-to-cumulus transition in the subtropical marine boundary layer (see Fig. 2). The ICA and 3D results using four solar zenith angles are presented. In the stratocumulus cases, the differences between the 3D and ICA calculations for the reflected and transmitted fluxes are smaller than 5 W m^{-2}. Errors in absorption due to the ICA are also small ($<$1.5 W m^{-2}). These results agree with previous studies (e.g., Cahalan et al. 1994b; Barker 1996) that show that the ICA works very well for domain-averaged fluxes of a marine stratocumulus cloud field.

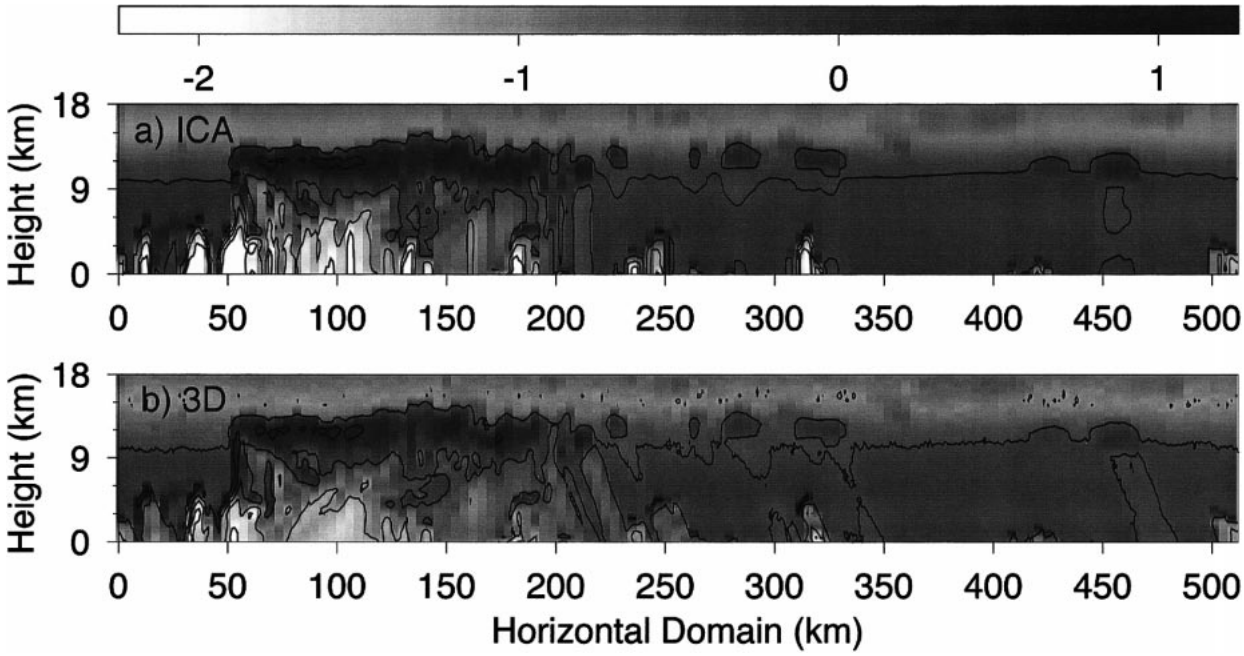

FIG. 5. Solar heating rates for the mature stage of a tropical cloud system using the (a) independent column approximation (ICA) and (b) 3D Monte Carlo scheme. The grayscale is linear to the logarithm of the heating rates. Contours shown are 0.01, 0.1, 1, and 10 K day^{-1}. The solar zenith angle is 60° and the surface albedo is 0.05.

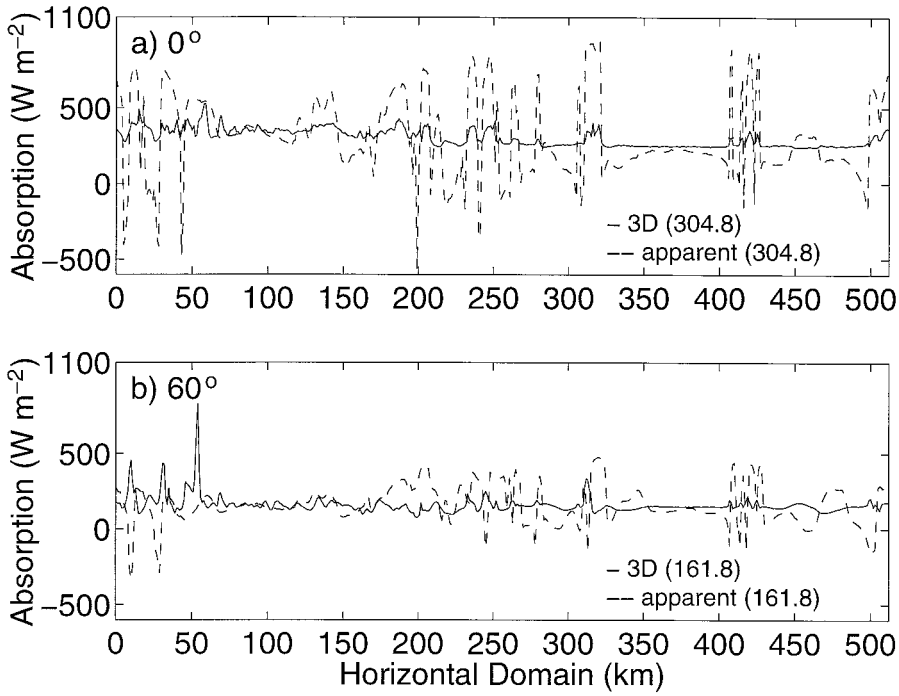

FIG. 6. The atmospheric column absorption as a function of the horizontal distance (km) for the mature stage of the tropical cloud field at solar zenith angles of (a) 0° and (b) 60°. The actual atmospheric absorption is from the 3D Monte Carlo simulation (solid line) and the apparent absorption (dashed line) is defined as the difference between the net fluxes at the top of the atmosphere and at the surface. Numbers in parentheses are the averages of the particular quantity over the horizontal domain.

TABLE 3. Domain-averaged solar upward fluxes at the top of the atmosphere ($\overline{F}^{\uparrow}_{\mathrm{TOA}}$), domain-averaged solar downward fluxes at the surface ($\overline{F}^{\downarrow}_{\mathrm{SFC}}$), and the domain-averaged absorption in the atmosphere for the Sc, Cu under Sc, and the trade Cu stages during the stratus-to-cumulus transition in the subtropical marine boundary layer. The ICA and 3D Monte Carlo calculations at different solar zenith angles (θ) are presented, along with the differences (Δ). Units are W m^{-2}.

		$\overline{F}^{\uparrow}_{\mathrm{TOA}}$			$\overline{F}^{\downarrow}_{\mathrm{SFC}}$			$\overline{A}$		
Cloud stages	θ	3D	ICA	$\Delta\overline{F}^{\uparrow}_{\mathrm{TOA}}$	3D	ICA	$\Delta\overline{F}^{\downarrow}_{\mathrm{SFC}}$	3D	ICA	$\Delta\overline{A}$
Sc	0	631.8	636.6	−4.8	360.6	356.1	4.5	385.9	385.4	0.5
	30	568.0	569.1	−1.1	282.9	281.7	1.2	341.3	341.3	0.0
	60	353.9	353.3	0.6	116.9	116.0	0.9	215.2	216.6	−1.4
	75	183.3	184.1	−0.8	42.9	41.4	1.5	128.0	128.6	−0.6
Cu under Sc	0	306.7	307.3	−0.6	774.6	774.8	−0.2	317.7	316.9	0.8
	30	289.6	291.7	−2.1	633.9	631.6	2.3	286.2	286.3	−0.1
	60	213.9	215.0	−1.1	288.0	286.8	1.2	192.6	192.7	−0.1
	75	128.1	127.1	1.0	110.0	110.7	−0.7	119.5	119.8	−0.3
Trade Cu	0	128.5	137.1	−8.6	1004.6	994.6	10.0	277.4	278.3	−0.9
	30	137.1	130.4	6.7	826.3	837.0	−10.7	256.0	252.5	3.5
	60	113.2	100.4	12.8	411.0	427.7	−16.7	176.5	173.4	3.1
	75	90.4	64.0	26.4	155.9	186.5	−30.6	113.6	110.9	2.7

For the trade cumulus cloud, differences in transmitted and reflected fluxes become significantly larger due to the effects of horizontal transport and cloud sides. For atmospheric absorption at nonzero solar zenith angles, the 3D results are ~3 W m^{-2} greater; this is attributed to the direct illumination of the lower cloud. With a solar zenith angle of 0°, the 3D case yields slightly less absorption. This can be explained by photon leakage from the clouds that decreases the heating rates in clouds. Figure 7 shows the comparison of domain-averaged heating rate profiles between the 3D and ICA simulations for the trade cumulus case. It is clearly shown that at the solar zenith angle of 0°, the heating rate decrease in clouds outweighs its increase below them; both are caused by the photon leakage from the clouds. At the solar zenith angle of 60°, we can see that the cloud side effect outweighs the shadowing effect. Figure 8 presents snapshots (x–z section) of the solar heating rates for the cumulus case at 60° from the ICA and 3D simulation. It can be seen that the increased heating at ~1 km for the 3D case (Fig. 7, for $\theta = 60°$) is because the dense cloud at 1 km is irradiated for 3D transfer but is in the shadow cast by the upper cloud for the ICA (Fig. 8). The tenuous cloud at ~1 km shows up clearly for the ICA but is in shadow for the 3D case. Obviously, more heating results from having the dense cloud at 1 km irradiated; hence the greater heating for 3D is shown in Fig. 7, when $\theta = 60°$.

For subtropical marine boundary clouds, the domain size we considered is only 5 km in extent. For the trade cumulus case, this domain only contains several cloud elements. So it may not be statistically meaningful to formulate general results on whether the ICA approach is valid in the broken-cumulus regime. But our results do show that for the trade cumulus cloud field, the 3D effects become more significant than those related to stratocumulus clouds.

5. Sensitivity of the effects of black carbon aerosol and water vapor continuum to cloud geometry

Many possible causes have been suggested for the often observed excess absorption in cloudy atmospheres (Stephens and Tsay 1990). These include the effects of black carbon absorbing aerosol and enhanced water vapor continuum absorption, as well as cloud 3D effects. Absorption by black carbon aerosol mainly occurs in the visible region (Chylek et al. 1984), while the water vapor continuum may contribute to atmospheric absorption in the near infrared (Chylek and Geldart 1997). Note that previous studies of aerosol and water vapor continuum effects were carried out within the plane-parallel framework of solar radiative transfer (e.g., Stephens and Tsay 1990).

Byrne et al. (1996) suggested that fields of broken clouds cause averaged photon pathlengths to be greater than those predicted by plane-parallel radiative transfer calculations, especially within and under cloud layers. Therefore, there is a possibility that black carbon within and below broken-cloud fields, and the water vapor continuum, which is largely confined in the lower atmosphere, may lead to significant enhanced absorption in realistic cloudy atmospheres. This section presents results pertaining to the impact of cloud geometry on the effects of black carbon aerosol and water vapor continuum.

a. Black carbon aerosol

Measurements of black carbon made near the surface and by aircraft suggest that typical black carbon concentrations several hundred miles away from major industrial or urban sources vary between 0.05 and 0.3 μg m^{-3} (Pinnick et al. 1993; Chylek et al. 1996). Typical black carbon concentrations near medium-sized urban areas are between 0.5 and 2 μg m^{-3}, while reported concentrations near major industrial or urban sources

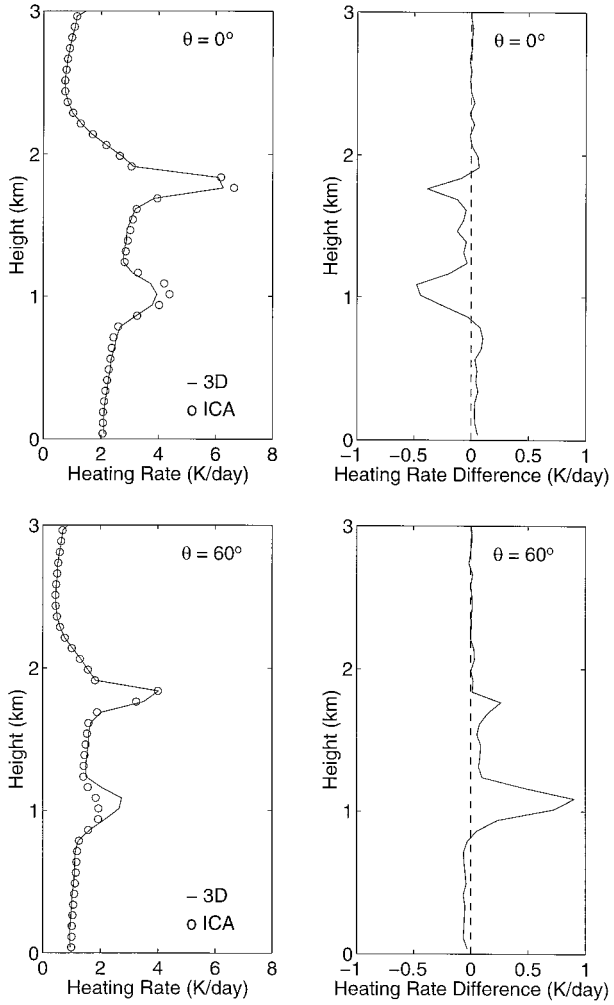

FIG. 7. (left) Domain-averaged solar heating rate profiles computed from the 3D Monte Carlo (3D) and independent column approximation (ICA) schemes using solar zenith angles of 0° and 60°; (right) the corresponding differences between the 3D and ICA calculations. The results are for the trade cumulus stage of a stratus-to-cumulus transition.

can be as large as 10 μg m^{-3}. In addition to industrial and urban sources, black carbon can also be produced by biomass burning. Recent data from aircraft observations in Nova Scotia, Canada, show that concentrations were increased from ~0.1 to ~1.0 μg m^{-3} by a forest fire in central Quebec, Canada; the smoke covered the Canadian Maritime Provinces and Maine on 22 August 1995 (P. Chylek 1997, personal communication).

In our sensitivity study, we assume a black carbon concentration of 0.6 μg m^{-3}. An aerosol layer is placed from 1 to 4 km in the tropical convective cloud system and from 0.5 to 2 km for the subtropical marine boundary cloud. The optical properties from d'Almeida et al. (1991) for the soot aerosol type are adopted. Using a black carbon density of 2 g cm^{-3} and a lognormal size distribution with the median radius of 0.0118 μm and a standard deviation of two (d'Almeida et al. 1991), we can derive the aerosol number density of ~5000 cm^{-3}.

Numerical results show that for the tropical convective cloud system at different stages with different solar zenith angles, black carbon aerosol increases domain-averaged atmospheric absorption by about 4–10 W m^{-2}. For the subtropical marine boundary cloud, the increase in atmospheric absorption is about 3–5 W m^{-2}. At low solar zenith angles, it is found that the ICA slightly underestimates the aerosol's effect on atmospheric absorption. This is because the ICA neglects the photon leakage from the cloud sides. At all solar zenith angles considered for both cloud systems, differences between the aerosol's effects estimated from the ICA and those from the 3D are less than 0.5 W m^{-2}.

b. Water vapor continuum

It has long been recognized that an empirical continuum absorption related to water vapor is required to interpret observed absorption in the infrared and microwave spectral regions (e.g., Stephens and Tsay 1990). Water vapor continuum absorption in the solar spectrum is likely, but its magnitude is uncertain due to lack of measurements. The water vapor continuum absorption may be due to the far wings of the water molecule absorption lines or due to water molecule polymers. Chylek and Geldart (1997) obtained the first estimate of atmospheric absorption of solar radiation by water vapor dimers. Tso et al. (1998) has provided a more extensive and detailed quantum mechanical calculation of the water vapor dimer absorption cross section. Chylek et al. (1999) discussed the water dimer concentration and the effect of dimers on atmospheric solar absorption.

In this study, Tso et al.'s (1998) water vapor dimer absorption cross sections are used. From Chylek et al. (1999), the dimer atmospheric concentrations based on various studies can differ by a factor of four. Herein, their C2 concentration is employed, which provides a median concentration.

Numerical results show that for different solar zenith angles, water vapor dimers enhance domain-averaged atmospheric absorption by about 6–20 W m^{-2} in the tropical convective cloud system. For the subtropical marine boundary cloud, the increase in absorption is from about 6–12 W m^{-2}. Since there is a large uncertainty in the dimer atmospheric concentration, the effect of dimers on the atmospheric solar absorption is still an open question (Fu et al. 1998). However, the focus here is to examine the sensitivity of the effect of water vapor continuum to cloud geometry. We find that cloud 3D effects only introduce differences less than 0.5 W m^{-2} in absorption due to the water vapor dimer. It is also found that the ICA slightly underestimates the dimer effect at solar noon but overestimates it at a large solar zenith angle, which is attributed to neglecting the effects of photon leakage and cloud slanted shadowing, respectively.

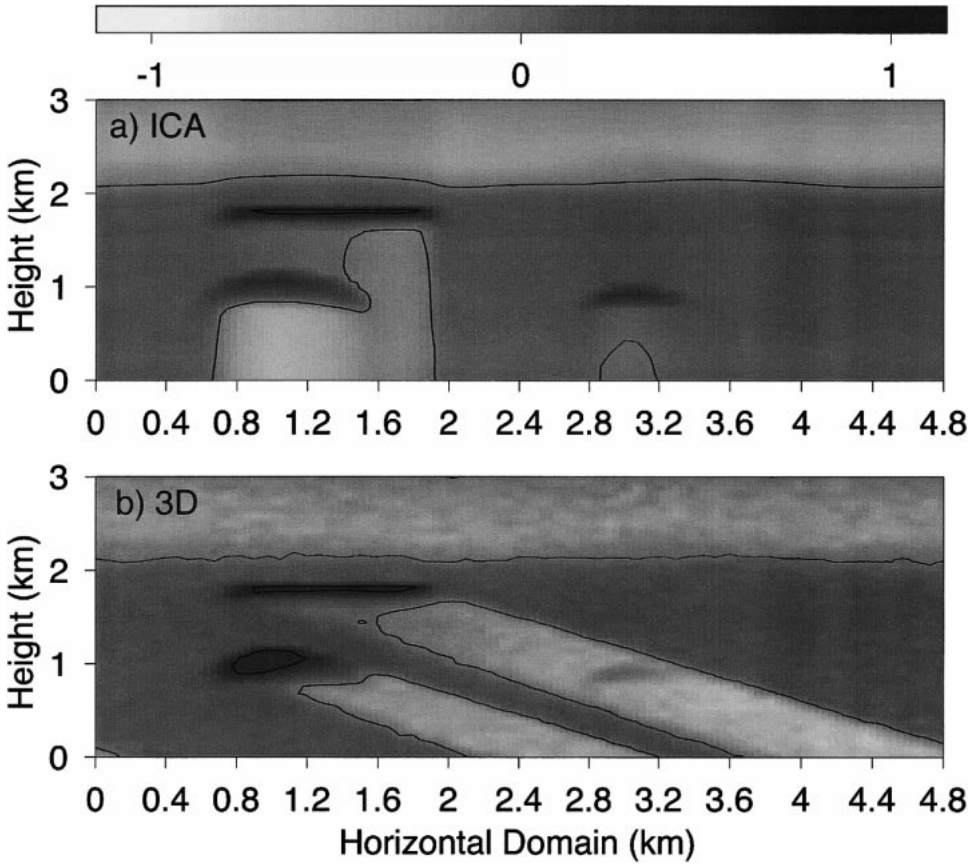

FIG. 8. Solar heating rates for the trade cumulus stage of a stratus-to-cumulus transition using the (a) independent column approximation (ICA) and (b) 3D Monte Carlo (3D) scheme. The grayscale is linear to the logarithm of the heating rates. Contours shown are 1 and 10 K day^{-1}. The solar zenith angle is 60° and the surface albedo is 0.05.

6. Summary and conclusions

This work aimed to improve the understanding of cloud 3D effects on atmospheric absorption of solar radiation. We have formulated a 3D broadband radiative transfer scheme by integrating a 3D Monte Carlo photon transport algorithm into the Fu–Liou radiation model. The validity of the mixing rule, which combines the optical properties due to gases and cloud hydrometeors, was examined. The 3D radiation model was applied to two-dimensional cloud fields generated by a cloud-resolving model. Two typical cloud systems, tropical deep convective clouds and subtropical marine boundary layer clouds, were considered. The cloud 3D effects on the radiative energy budget were examined by comparing the 3D results with those from the independent column approximation (ICA), which applies the plane-parallel radiation model to each column of the cloud field.

For the tropical convective cloud system, it was found that cloud 3D effects always enhance atmospheric absorption regardless of the solar zenith angle. In a large horizontal domain (512 km), differences in domain-averaged atmospheric solar absorption between the 3D and ICA are less than 4 W m^{-2}. However, considering a smaller domain (e.g., 75 km) containing a cluster of deep convective towers, domain-averaged absorption can be enhanced by more than 20 W m^{-2} in the daytime. It was also shown that the ICA underestimates transmitted fluxes for overhead sun due to neglect of photon leakage from cloud sides. For low sun, the ICA underestimates reflected fluxes because of neglecting direct illumination of cloud sides. In the 3D case, cloud sides increase the effective cloud cover as solar zenith angle increases.

For a subtropical marine boundary cloud system during the stratus-to-cumulus transition, it was shown that the ICA works very well for domain-averaged absorption and fluxes of a stratocumulus cloud field. In the trade cumulus case, cloud geometry has a more pronounced impact.

The effects of black carbon aerosol and the water vapor continuum on atmospheric absorption were also examined. Of particular concern was the sensitivity of these effects to cloud geometry. It was shown that the effects of black carbon aerosol and water vapor continuum estimated from the ICA differ from those based on the 3D radiation model by less than 0.5 W m^{-2}.

The current study indicates that the atmospheric absorption enhancement due to cloud-related 3D photon transport is small, which could not explain the excess absorption suggested by recent studies. It is also suggested, however, that the cloud 3D effects have to be considered very carefully in order to estimate the atmospheric absorption using the differences of net fluxes.

Acknowledgments. The research work contained herein has been supported by DOE Grant DE-FG02-97ER62363 and, in part, by NSERC Operating Grant and NSERC Collaborative Grant.

REFERENCES

Albrecht, B. A., D. A. Randall, and S. Nicholls, 1988: Observations of marine stratocumulus clouds during FIRE. *Bull. Amer. Meteor. Soc.,* **69,** 618–626.

Arking, A., 1996: Absorption of solar energy in the atmosphere: Discrepancy between model and observations. *Science,* **273,** 779–782.

Barker, H. W., 1991: Soalr radiative fluxes for realistic extended broken cloud fields above reflecting surfaces. Ph.D. thesis, McMaster University, 257 pp. [Available from University Microfilm, 305 N. Zeeb Rd., Ann Arbor, MI 48106.]

——, 1996: Estimating cloud field albedo using one-dimensional series of optical depth. *J. Atmos. Sci.,* **53,** 2826–2837.

——, and Q. Fu, 1999: Modeling domain-averaged solar fluxes for an evolving tropical cloud system. *Atmos. Oceanic Opt.,* **12,** 211–217.

——, J. J. Morcrette, and G. D. Alexander, 1998: Broadband solar fluxes and heating rates for atmospheres with 3D broken clouds. *Quart. J. Roy. Meteor. Soc.,* **124,** 1245–1271.

Barkstrom, B. R., 1984: The Earth Radiation Budget Experiment (ERBE). *Bull. Amer. Meteor. Soc.,* **65,** 1170–1185.

Byrne, R. N., R. C. J. Somerville, and B. Subasilar, 1996: Broken-cloud enhancement of solar radiation absorption. *J. Atmos. Sci.,* **53,** 878–886.

Cahalan, R. F., W. Ridgeway, W. J. Wiscombe, T. L. Bell, and J. B. Snider, 1994a: The albedo of fractal stratocumulus clouds. *J. Atmos. Sci.,* **51,** 2434–2455.

——, ——, ——, S. Gollmer, and Harshvardhan, 1994b: Independent pixel and Monte Carlo estimates of stratocumulus albedo. *J. Atmos. Sci.,* **51,** 3776–3790.

Cess, R. D., and Coauthors, 1995: Absorption of solar radiation by clouds: Observations versus models. *Science,* **267,** 496–499.

Chylek, P., and D. J. W. Geldart, 1997: Water vapor dimers and atmsopheric absorption of electromagnetic radiation. *Geophys. Res. Lett.,* **24,** 2015–2018.

——, V. Ramaswamy, and R. J. Cheng, 1984: Effect of graphitic carbon on the albedo of clouds. *J. Atmos. Sci.,* **41,** 3076–3084.

——, and Coauthors, 1996: Black carbon: Atmospheric concentrations and cloud water content measurements over southern Nova Scotia. *J. Geophys. Res.,* **101,** 29 105–29 110.

——, Q. Fu, H. C. W. Tso, and D. J. W. Geldart, 1999: Contribution of water vapor dimers to clear sky absorption of solar radiation. *Tellus,* **51A,** 304–313.

d'Almeida, G., P. Koepke, and E. P. Shettle, 1991: *Atmospheric Aerosols—Global Climatology and Radiative Characteristics.* A. Deepak, 561 pp.

Fu, Q., 1991: Parameterization of radiative processes in vertically nonhomogeneous multiple scattering atmospheres. Ph.D. dissertation, University of Utah, 259 pp. [Available from University Microfilm, 305 N. Zeeb Rd., Ann Arbor, MI 48106.]

——, and K. N. Liou, 1992: On the correlated *k*-distribution method for radiative transfer in nonhomogeneous atmospheres. *J. Atmos. Sci.,* **49,** 2139–2156.

——, and ——, 1993: Parameterization of the radiative properties of cirrus clouds. *J. Atmos. Sci.,* **50,** 2008–2025.

——, S. K. Krueger, and K. N. Liou, 1995: Interactions between radiation and convection in simulated tropical cloud clusters. *J. Atmos. Sci.,* **52,** 1310–1328.

——, G. Lesins, J. Higgins, T. Charlock, P. Chylek, and J. Michalsky, 1998: Broadband water vapor absorption of solar radiation tested using ARM data. *Geophys. Res. Lett.,* **25,** 1169–1172.

Kiehl, J. T., J. J. Hack, M. H. Zhang, and R. D. Cess, 1995: Sensitivity of a GCM climate to enhanced shortwave cloud absorption. *J. Climate,* **8,** 2200–2212.

Krueger, S. K., 1988: Numerical simulation of tropical cumulus clouds and their interaction with the subcloud layer. *J. Atmos. Sci.,* **45,** 2221–2250.

——, G. T. McLean, and Q. Fu, 1995: Numerical simulation of the stratus-to-cumulus transition in the subtropical marine boundary layer. Part I: Boundary-layer structure. *J. Atmos. Sci.,* **52,** 2839–2850.

Kyle, H. L., and Coauthors, 1993: The Nimbus Earth Radiation Budget (ERB) Experiment: 1975 to 1992. *Bull. Amer. Meteor. Soc.,* **74,** 815–830.

Li, Z., K. Masuda, and T. Takashima, 1993: Estimation of SW flux absorbed at the surface from TOA reflected flux. *J. Climate,* **6,** 317–330.

——, H. W. Barker, and L. Moreau, 1995: The variable effect of clouds on atmospheric absorption of solar radiation. *Nature,* **376,** 486–490.

Liou, K. N., Q. Fu, and T. P. Ackerman, 1988: A simple formulation of the delta-four-stream approximation for radiative transfer parameterizations. *J. Atmos. Sci.,* **45,** 1940–1947.

Mace, G. G., T. P. Ackerman, P. Minnis, and D. F. Young, 1998: Cirrus layer microphysical properties derived from surface-based millimeter radar and infrared interferometer data. *J. Geophys. Res.,* **103,** 23 207–23 216.

McClatchey, R. A., R. W. Fenn, J. E. A. Selby, F. E. Volz, and J. S. Garing, 1971: Optical properties of the atmosphere. Air Force Rep. AFCRL-71-0279, 85 pp. [Available from Air Force Geophysics Laboratory, Bedford MA 01731.]

O'Hirok, W., and C. Gautier, 1998: A three-dimensional radiative transfer model to investigate the solar radiation within a cloudy atmosphere. Part I: Spatial effects. *J. Atmos. Sci.,* **55,** 2162–2179.

Pilewskie, P., and F. Valero, 1995: Direct observations of excess solar absorption by clouds. *Science,* **257,** 1626–1629.

Pinnick, R. G., G. Fernandez, E. Martinez-Andazola, B. D. Hinds, A. D. A. Hansen, and K. Fuller, 1993: Aerosol in the arid southwestern United States: Measurements of mass loading, volatility, size distribution, absorption characteristics, black carbon content, and vertical structure to 7 km above sea level. *J. Geophys. Res.,* **98,** 2651–2666.

Ramanathan, V., and Coauthors, 1995: Warm pool heat budget and shortwave cloud forcing: A missing physics. *Science,* **267,** 499–503.

Stephens, G. L., 1996: How much solar radiation do clouds absorb? *Science,* **271,** 1131–1133.

——, and S. C. Tsay, 1990: On the cloud absorption anomaly. *Quart. J. Roy. Meteor. Soc.,* **116,** 671–704.

Tso, H. C. W., D. J. W. Geldart, and P. Chylek, 1998: Effects of unharmonicity on the water vapor dimer absorption cross section. *J. Chem. Phys.,* **108,** 5319–5329.

Welch, R. M., and B. A. Wielicki, 1984: Stratocumulus cloud field reflected fluxes: The effect of cloud shape. *J. Atmos. Sci.,* **41,** 3085–3103.

Wiscombe, W. J., 1995: An absorbing mystery. *Nature,* **376,** 466–467.

Xu, K. M., and S. K. Krueger, 1991: Evaluation of cloudiness parameterizations using a cumulus ensemble model. *Mon. Wea. Rev.,* **119,** 342–367.

Zuidema, P., and K. F. Evans, 1998: On the validity of the independent pixel approximation for boundary layer clouds observed during ASTEX. *J. Geophys. Res.,* **103,** 6059–6074.